

See discussions, stats, and author profiles for this publication at: <https://www.researchgate.net/publication/43245751>

A Nonheme High-Spin Ferrous Pool in Mitochondria Isolated from Fermenting *Saccharomyces cerevisiae*

ARTICLE *in* BIOCHEMISTRY · MAY 2010

Impact Factor: 3.02 · DOI: 10.1021/bi1001823 · Source: PubMed

CITATIONS

20

READS

9

6 AUTHORS, INCLUDING:



Gregory Holmes-Hampton

National Institutes of Health

12 PUBLICATIONS 153 CITATIONS

SEE PROFILE



Yisong Guo

Carnegie Mellon University

31 PUBLICATIONS 492 CITATIONS

SEE PROFILE

Published in final edited form as:

Biochemistry. 2010 May 18; 49(19): 4227–4234. doi:10.1021/bi1001823.

A Nonheme High-Spin Ferrous Pool in Mitochondria Isolated from Fermenting:

Saccharomyces cerevisiae †

Gregory P. Holmes-Hampton¹, Ren Miao¹, Jessica Garber-Morales¹, Yisong Guo², Eckard Münck², and Paul A. Lindahl^{1,3,*}

¹Department of Chemistry, Texas A&M University, College Station, TX 77843-3255

²Department of Chemistry, Carnegie Mellon University, Pittsburgh, PA 15213

³Department of Biochemistry and Biophysics, Texas A&M University, College Station, TX 77843

Abstract

Mössbauer spectroscopy was used to detect pools of Fe in mitochondria from fermenting yeast cells, including those consisting of nonheme high-spin (HS) Fe^{II} species, Fe^{III} nanoparticles, and mononuclear HS Fe^{III} species. At issue was whether these species were located within mitochondria or were exterior to it. None could be removed by washing mitochondria extensively with ethylene glycol tetraacetic acid or bathophenanthroline sulfonate (BPS), Fe^{II} chelators that do not appear to penetrate mitochondrial membranes. However, when mitochondrial samples were sonicated, BPS coordinated the Fe^{II} species, forming a low-spin Fe^{II} complex. This treatment also diminished both Fe^{III} species, suggesting that all of these Fe species are encapsulated by mitochondrial membranes and are protected from chelation until membranes are disrupted. 1,10-phenanthroline (phen) is chemically similar to BPS but is membrane soluble; it coordinated nonheme HS Fe^{II} in unsonicated mitochondria. Further, the HS Fe^{III} species and nanoparticles were not reduced by dithionite until the detergent deoxycholate was added to disrupt membranes. There was no correlation between the percentage of nonheme HS Fe^{II} species in mitochondrial samples and the level of contaminating proteins. These results collectively indicate that the observed Fe species are contained within mitochondria. Mössbauer spectra of whole cells were dominated by HS Fe^{III} features; the remainder displayed spectral features typical of isolated mitochondria, suggesting that the Fe in fermenting yeast cells can be coarsely divided into two categories: mitochondrial Fe and (mostly) HS Fe^{III} ions in one or more non-mitochondrial locations.

Iron serves critical roles in cell biology, generally involving catalytic and redox processes. This transition metal is found in many prosthetic groups, including hemes and iron sulfur clusters. These groups typically serve as enzyme active sites and redox centers. Dysfunction in cellular iron metabolism has been implicated in aging and in the pathogenesis of diseases involving reactive oxygen species (1). Clearly, cells *need* iron but they must handle it carefully to avoid

†This study was supported by the National Institutes of Health grants GM084266, (PAL), EB-001475 (EM), T32GM008523 (GPHH and JGM) and the Robert A. Welch Foundation (A1170, PAL).

*To whom correspondence should be addressed: Phone: 979-845-0956; FAX: 979-845-4719; lindahl@chem.tamu.edu.

Supporting Information Available: Fig. S1, Western blot of isolated mitochondria; Fig. S2, Mössbauer spectra of EGTA-washed mitochondria from fermenting cells; Fig. S3, effect of sonication; Fig. S4, the third BPS experiment; Fig. S5, Western blot of eight independent mitochondria preparations; Fig. S6, effect of deoxycholate on Mössbauer spectra of dithionite-reduced mitochondria; Fig. S7, Mössbauer spectrum of whole fermenting yeast cells after sonication and treatment with dithionite. This material is available free of charge via the Internet at <http://pubs.acs.org>.

being damaged by it. Deciphering how cells do this will require a better understanding of iron *trafficking* in cells.

Mitochondria are traffic “hubs”, used to assemble Fe/S clusters and synthesize hemes. In yeast, the Fe^{II} ions that are used as feedstock for these processes are imported into the matrix through the high-affinity inner membrane transporters Mrs3p and Mrs4p (2). The ligands coordinating these species have been hypothesized to be non-proteinaceous and of low molecular weight (3). The matrix-localized yeast frataxin homolog protein Yfh1p apparently shuttles these ions to the scaffold protein Isu1p for Fe/S assembly, and perhaps to ferrochelatase for heme biosynthesis (4).

Starting with studies by Flatmark and Tangerås (5), efforts have been made to characterize the low molecular weight mononuclear nonheme Fe species in mitochondria. By exposing the organelles to BPS, a strong chelator of mononuclear Fe^{II} ions, they estimated that ~ 25% of mitochondrial Fe is present as a chelatable or *labile* Fe pool.

Recent fluorescence-based studies in mitochondria from rat hepatocytes indicate a far lower concentration of chelatable Fe. Petrat *et al.* (6,7) incubated cells with fluorescent indicators that accumulate in mitochondria. Fe binding causes fluorescence quenching, and so the presence of residual fluorescence in their samples indicated that the binding reaction was limited by the Fe in mitochondria rather than by the indicator. Subsequent addition of the tight-binding non-fluorescent chelator phen penetrated the mitochondria and replaced the Fe bound indicator thereby causing fluorescence recovery. The extent of recovery indicated that the concentration of chelatable Fe in rat liver mitochondria was 12 – 17 μ M. The authors estimated that the chelatable Fe pool corresponded to just ~ 0.4% of the total Fe in the organelle. They attributed Tangerås’ dramatically higher estimate to adventitious Fe generated during the isolation of the organelle.

As explained by Petrat *et al.* (6), the fluorescence/chelator-based approach for quantifying Fe complexes in mitochondria within a cell is superior to directly measuring Fe in isolated mitochondria. This is so because cells need not be disrupted for these experiments, such that adventitious Fe is not generated. However, this approach *is* disruptive in another sense – it destroys the Fe complexes of interest as an inherent part of the detection process. Methods that would allow such complexes to be detected *without* destroying them would have a distinct advantage, as they could facilitate the eventual isolation and characterization of such complexes. Of course, any such method would be useful only if adventitious Fe could be distinguished from Fe that is functionally associated with mitochondria. In this study, we describe the use of Mössbauer spectroscopy to detect three pools of Fe in mitochondria from fermenting yeast cells, including nonheme high-spin (NHHS) Fe^{II} species, magnetically isolated (i.e non-interacting) mononuclear HS Fe^{III} species, and Fe^{III} nanoparticles. The major objective of this study was to establish whether these Fe-containing species are located *within* the mitochondria (where they might serve a metabolic role), or on the *exterior* of the organelle (where they would be simply artifacts of our isolation procedure, and counted as adventitiously-bound iron). Our results indicate that they are indeed located inside mitochondria.

Experimental Procedures

Cell Growth and mitochondria isolation

25L cultures of W303-1B cells were grown on Fe-deficient minimal media supplemented with 40 μ M ⁵⁷Fe (8). Cells were harvested at OD₆₀₀ = 1.0-1.4 and then transferred to a glovebox (~6 °C, ~1 ppm O₂). Mitochondria were isolated anaerobically as described (8-10), except that cells were treated with ~1000 units lyticase/g wet cells for ~50 min. Also, cells were disrupted

with 20-25 strokes of the Dounce homogenizer, and a 14.5 - 18.5%-Nycodenz gradient was used. In some experiments, the re-suspension buffer contained chelators and/or dithionite (10 mM final concentration). Samples isolated with buffers that included 1 mM EGTA are referred to as EGTA-washed mitochondria. Mössbauer spectra were collected and analyzed as described (8).

Western blots were obtained using specific antibodies for cellular organelles, including mitochondrial porin (Invitrogen), the vacuolar protein carboxypeptidase Y (CPY; Invitrogen), the cytosolic protein 3-phosphoglycerate kinase (PGK; Invitrogen) and the endoplasmic reticular protein Kar2 (Santa Cruz Biotechnology). Goat anti-mouse HRP conjugate secondary antibodies (Invitrogen) were used with all primary antibodies except Kar2, which used goat anti-rabbit HRP conjugate secondary antibody (Santa Cruz Biotechnology). Thermo Scientific Enhanced Chemiluminescent (ECL) Western Blotting Substrate (Thermo Scientific) was then added. Images were obtained (FujiFilm LAS-4000mini) with a 10 sec standard exposure and the chemiluminescence setting. Images were analyzed using the MultiGuage v3.1 software.

BPS experiments

In the first and third experiments, cells were treated with buffers containing 1 mM EGTA for the initial steps, including those used to rinse the cells and for incubation with lyticase. The buffer used just prior to homogenization and in all steps thereafter contained 3 mM BPS. Past the step in which mitochondria were collected from the density gradients, all buffers included dithionite 10 mM. The mitochondrial sample was rinsed and packed into a Mössbauer sample holder which was then frozen anaerobically. Spectra were collected and the sample was thawed anaerobically and sonicated 5×15 sec with a Branson 450 sonifier at a 60% duty load using a two-step microtip. The sample was then refrozen anaerobically and the Mössbauer spectrum was re-collected. In the second and fourth experiments (Fig. 2, C and D, and Fig. S4), mitochondria were collected with EGTA in all buffers. In the step just prior to being frozen, the sample was treated with buffer containing 3 mM BPS. Dithionite was also included in the fourth experiment.

Phenanthroline experiment

EGTA-washed mitochondria were split into two aliquots; one was left untreated, the other was treated with 3 mM phen (ACROS Organics). After 30 min, both were packed into Mössbauer cups and frozen anaerobically.

Dithionite and Deoxycholate experiment

A sample of EGTA-washed mitochondria was split equally and treated with dithionite (10 mM final). One half was treated with deoxycholate (ACROS Organics) (0.5%, final). Samples were frozen after 30 min incubation in the glovebox.

Whole cells

Cells were grown on minimal media under constant shaking, and harvested at an OD₆₀₀ of 1.0. Cells were collected by centrifugation at 4000×g and rinsed with unbuffered 100 μM ethylenediaminetetraacetic acid. Cells were rinsed twice with water, packed into a Mössbauer sample holder, and frozen. After collecting spectra, cells were thawed anaerobically, sonicated as above, and refrozen.

Results

All samples of mitochondria were anaerobically isolated from fermenting yeast cells. This involved numerous steps in which samples were suspended in buffer, pelleted by

centrifugation, and then resuspended in fresh buffer after discarding the supernatant. We refer to these steps as *washing*. Mitochondria were initially washed with buffers that did *not* include metal chelators. Such preparations exhibited at low-temperature (4.5 K) and in weak applied magnetic fields (0.05 T) Mössbauer spectra possessing quadrupole doublets typical of nonheme high-spin (NHHS) Fe^{II} species. Such doublets had been observed in spectra of mitochondria isolated from WT respiring (lactate-grown) cells (9). The major objective of the current study was to establish whether these Fe^{II} ions were located *within* fermenting mitochondria, where they might serve a metabolic role, or located on the *exterior* of the organelle, in which case they would probably be artifacts of our isolation procedure.

Throughout these studies, mitochondrial purity was an important consideration. Western blot analysis of our isolated mitochondria indicated a $\sim 30\times$ enrichment of the mitochondrial porin relative to the amount present in cell extracts (Fig. S1). In fermenting cells, mitochondria occupy $\sim 3\%$ of the cellular volume (11), suggesting that our preparations were relatively pure. Western blot analysis indicated some contaminating vacuolar, endoplasmic reticular and cytosolic proteins, as is generally observed (10).

Samples were packed by centrifugation into Mössbauer holders (an open delrin cup) to maximize the amount of Fe examined. However, the resulting spectra (Fig. 1) had lower S/N ratios than is readily obtained with Fe-containing proteins or small molecules, due to the low inherent concentration of Fe in mitochondria (700 – 800 μM Fe overall and typically 200 – 300 μM of ^{57}Fe in samples grown on ^{57}Fe -enriched media). In spectra of mitochondria, the quality was sufficient to recognize some minor species ($\geq \sim 10\%$), but insufficient to quantify such species to greater than $\pm 5\%$ precision.

Nonheme high-spin (NHHS) Ferrous Ions in EGTA-Washed Fermenting Mitochondria

Our initial strategy was to remove adventitiously bound NHHS Fe^{II} by including 1 mM EGTA, a strong Fe^{II} chelator, in all washing buffers used during mitochondrial isolation. Such samples were exposed to the chelator for ~ 6 hrs overall. In the packing step, all EGTA of the final wash was removed except for that residing between the packed mitochondrial particles (the residual buffer was previously estimated to occupy $\sim 20\%$ of total volume (9,12). This quantity of residual EGTA was sufficient to coordinate $\sim 200 \mu\text{M}$ Fe^{II} ions. We chose EGTA because it reportedly does not penetrate mitochondrial membranes (13). Also, the Fe^{II} EGTA quadruple doublet can be distinguished reasonably well from the NHHS Fe^{II} doublet associated with our mitochondria samples. Despite these efforts, the nonheme, non- Fe^{II} (EGTA) HS Fe^{II} doublet was observed in all of the ~ 30 independently-prepared batches of EGTA-washed mitochondria examined. Spectra of 4 other batches (Fig. S2) illustrate the extent of batch-to-batch variation.

The blue line in Fig. 1A is a simulation assuming isomer shift, quadrupole splitting and effective linewidth parameters of $\delta \approx 1.25$ mm/s, $\Delta E_Q \approx 3.35$ mm/s, and $\Gamma = -0.65$ mm/s, respectively (in WMOSS, a negative linewidth indicates a Voigt profile with a Lorentzian of 0.15 mm/s full width convoluted into a Gaussian with $\sigma = -0.65$ mm/s). These values are typical of mononuclear $\{\text{Fe}^{2+}(\text{O})_m(\text{N})_n\}$ complexes for which $5 \leq (m+n) \leq 6$ and $m \geq 4$ (14). HS Fe^{II} hemes have parameters δ ranging from 0.92–0.95 mm/s and ΔE_Q ranging from 2.02 to 2.20 mm/sec (15,16). The low-energy absorption line of the NHHS Fe^{II} doublet is hidden within the central doublet (see below) while the high-energy line, which contains half of the doublet's intensity, is generally resolved. This line is marked by the arrow in Fig. 1A and in all other spectra. In Fig. 1A, the spectral area of the doublet represents 20% of the Fe in the sample, corresponding to $\sim 150 \mu\text{M}$ Fe^{II} . The large width of the absorption lines suggests multiple species. This experiment shows that the NHHS Fe^{II} ions in our sample are protected from EGTA chelation despite extensive washing of mitochondria with EGTA-containing buffers.

Mössbauer spectra of fermenting mitochondria also contain a quadrupole doublet representing ~20% of the total Fe, with $\delta = 0.45$ mm/s and $\Delta E_Q \sim 1.15$ mm/s. This species, called the *central doublet*, arises from unresolved $S = 0$ $[\text{Fe}_4\text{S}_4]^{2+}$ clusters and low-spin ferrous hemes (Fig. 1A, red line) (8,9). In strong applied fields the contribution of these species can readily be simulated (Fig. 1C, blue line) because the effective field at the nucleus arises solely from the applied field. In contrast, HS Fe^{II} ions exhibit paramagnetic hyperfine structure spread over a wide velocity range, making it difficult to characterize in 8.0 T spectra.

EGTA-washed fermenting mitochondria also exhibited spectral features from magnetically isolated high-spin ($S = 5/2$) mononuclear Fe^{III} species with $E/D \sim 1/3$. In weak applied fields (0.05 T), magnetically isolated Fe^{III} yield intricate Mössbauer patterns exhibiting paramagnetic hyperfine structure. With the low ^{57}Fe concentrations in these samples, such features cannot be analyzed well or easily distinguished from baseline (distorting the quantification of other species). Fortunately in 8 T applied fields, the outmost features of HS Fe^{III} components are resolved (Fig. 1C, red line), allowing an accurate estimate of concentration (here 20% of spectral intensity, corresponding to ~ 150 μM Fe).

In 0.05 T applied fields, and at 4.5 K (Fig. 1A) and 100 K (Fig. 1B), EGTA-washed fermenting mitochondria also yielded a quadrupole doublet with $\Delta E_Q \approx 0.63$ mm/s and $\delta \approx 0.52$ mm/s; the red line in Fig. 1B. Similar doublets were present in spectra of mitochondria isolated from Yfh1p-, Yah1p-, and Atm1p-depleted cells (4,8,17); they arise from Fe^{III} phosphate nanoparticles exhibiting superparamagnetism. In strong applied fields, these nanoparticles yield broad unresolved features (see Fig. 2D of (8)). Quantification is most accurate at temperatures well above the blocking temperature, T_B ; for $T \gg T_B$, spectra consist of a quadrupole doublet (in the present samples, $T_B < 4.2$ K). The 100 K spectrum (Fig. 1B) shows that $\sim 40\%$ of the Fe of the sample belongs to Fe^{III} nanoparticles.

In summary, the Fe in EGTA washed fermenting WT mitochondria is distributed into 4 major groups. Approximately 20% is NHHS Fe^{II} , $\sim 20\%$ is a combination of $[\text{Fe}_4\text{S}_4]$ and LS Fe^{II} hemes, $\sim 40\%$ Fe^{III} resides in nanoparticles, and $\sim 20\%$ is non-interacting mononuclear high-spin Fe^{III} . These organelles also contain small amounts of other Fe-containing species(18). All of these Fe-containing species were present despite extensive exposure of the mitochondria to a strong Fe^{II} chelator, suggesting that they are located within the organelle and protected from chelation.

BPS-treated mitochondria

As the difference in the positions of the high energy lines of the NHHS Fe^{II} doublet and the Fe^{II} EGTA doublet is modest, we wanted more compelling evidence that the NHHS Fe^{II} species in our samples were located within the organelle. BPS is orders-of-magnitude stronger than EGTA in terms of Fe^{II} chelation, and its negative charge should also make it impenetrable to mitochondrial membranes. However, the major advantage of using BPS is that it forms a LS Fe^{II} complex which is easily distinguishable from HS Fe^{II} ions.

The blue line in Fig. 2A is a 4.5 K Mössbauer spectrum of a mitochondria sample washed with 3 mM BPS. It contains a NHHS Fe^{II} doublet representing 20% of total iron. After collecting this spectrum, the sample was thawed, sonicated and re-frozen, all in a glove box containing ~ 1 ppm O_2 . The resulting spectrum (Fig. 2A hash marks) lacked the NHHS Fe^{II} doublet; rather, it exhibited a doublet with parameters $\Delta E_Q = 0.32$ mm/s and $\delta = 0.38$ mm/s indicating LS $\text{Fe}^{\text{II}}(\text{BPS})_3$. These changes are best visualized by the after-minus-before sonication difference spectrum shown in Fig. 2B. Features pointing upward (downward) are present before (after) sonication; unchanged features cancel. The spectral simulation (red line) assumes that 23% of the Fe in the sample converted to $\text{Fe}^{\text{II}}(\text{BPS})_3$ by sonication, including NHHS Fe^{II} (13%) and the central doublet (10%) (percentage in parentheses refers to total Fe, not % change of the

spectral species). The change corresponds to the majority of the initial NHHS Fe^{II} species and to about half of the central doublet. Other experiments suggest that sonication alone can destroy [Fe₄S₄]²⁺ clusters (Fig. S3), whereas BPS does not chelate Fe^{II} coordinated in heme centers (19). We suspect that sonication degraded a large portion of mitochondrial [Fe₄S₄] clusters and that the released Fe ions were reduced by endogenous agents present in mitochondria (or generated upon sonication) to Fe^{II} and coordinated by BPS.

Similar results were observed in a second independent experiment (Fig. 2, C and D) in which BPS was added to EGTA-washed mitochondria only in the final isolation step. Again, the majority of NHHS Fe^{II} ions and half of the central doublet were replaced by Fe^{II}(BPS)₃ after sonication. In this experiment, the majority of the iron contained in the Fe^{III} nanoparticles was also converted to Fe^{II}(BPS)₃ upon sonication (the first experiment showed a lower % of nanoparticles). We suspect that sonication released species (sulfide ions?) that reduced the Fe^{III} ions of the nanoparticles to HS Fe^{II} ions that were then coordinated by BPS. A third independent experiment (Fig. S4) using BPS-washed mitochondria also showed the semi-quantitative conversion of NHHS Fe^{II} ions into LS Fe^{II}(BPS)₃ upon sonication. Other Fe-containing species in the mitochondria also converted to Fe^{II}(BPS)₃ but our spectra are insufficiently resolved to identify them. A fourth experiment was conducted in which membranes were disrupted by exposure to deoxycholate rather than by sonication. This detergent has been used to disrupt mitochondrial membranes (22). The spectra, also shown in Fig. S4, again shows the presence of NHHS Fe^{II} in the BPS-washed sample, and the replacement of this doublet by the Fe^{II}(BPS)₃ doublet in the spectra of the sample treated with deoxycholate. The results of these four experiments establish that the NHHS Fe^{II} ions in our samples were protected from BPS chelation prior to sonication, and that they became susceptible to chelation after sonication. We conclude that this protection arose because these ions are encapsulated by the mitochondrial membrane across which BPS cannot penetrate. Sonication (or deoxycholate) disrupts these membranes, rendering the NHHS Fe^{II} ions accessible to chelation. Depending on the extent of BPS exposure, a portion of the Fe in [Fe₄S₄]²⁺ clusters and/or Fe-nanoparticles can also be chelated by BPS.

Mitochondria treated with Phenanthroline

From the perspective of Fe coordination, phen and BPS have the same structure and properties; both are extremely strong bidentate chelators that bind HS Fe^{II} to form LS Fe^{II} complexes. However, in contrast to negatively-charged BPS, phen is neutral and able to penetrate the mitochondrial inner membrane (IM) (6). Thus, if the NHHS Fe^{II} species are inside mitochondrial membranes, phen should chelate these ions in *unsonicated* mitochondria. To test this, an EGTA-washed mitochondria sample was divided in two; half was frozen without treatment and the other half was treated with phen and then frozen. The untreated control (Fig. 3A, blue line) is that of Fig. 1; it exhibited a HS Fe^{II} doublet representing 20% of the Fe in the sample. The matched phen-treated sample (Fig. 3A, black hash marks) lacked the NHHS Fe^{II} doublet but contained an intense quadrupole doublet with $\Delta E_Q = 0.31$ mm/s, $\delta = 0.37$ mm/s. These parameters are characteristic of LS Fe^{II}(phen)₃. This doublet represented 25% of the total Fe in the sample. These changes are illustrated in the “after-minus-before” difference spectrum (Fig. 3B). The red line is a simulation showing 15% NHHS Fe^{II} ions (the features pointing upward) converting to Fe^{II}(phen)₃ after exposure to phen. Some additional Fe species, representing ~10% of total Fe, also converted to Fe^{II}(phen)₃. These species exhibit the upward feature at ~1.2 mm/s in Fig. 3B. They might be Fe^{III} nanoparticles or Fe of the central doublet, but the spectra lack sufficient resolution to distinguish these. Phen did not cause the decline of the mononuclear HS Fe^{III} species, perhaps due to the weaker coordination of phen to ferric ions. Regardless, our main conclusion is that phen penetrates unsonicated mitochondria and coordinates the NHHS Fe^{II} ions located therein.

No correlation of NHHS Fe^{II} to contamination levels

One difficulty in determining the cellular location of the observed NHHS Fe^{II} species has been to exclude the possibility that they are encapsulated by membranes other than those of mitochondria. As has been discussed (10,20), the best method available for isolating large quantities of mitochondria (i.e. discontinuous density gradient centrifugation) does not remove all non-mitochondrial membranous material; the most common contaminants include endoplasmic reticulum (ER) and vacuoles (10). Besides having a density similar to that of mitochondria, the ER physically interacts with mitochondria for phospholipid biosynthesis and calcium signaling (21). These interactions might prevent the clean separation of the two organelles.

We have discovered that the % of NHHS Fe^{II} differs in mitochondria isolated from cells grown on different carbon sources (18). In mitochondrial preparations isolated from cells grown on glucose, galactose and glycerol, the NHHS Fe^{II} doublet quantified to 16%, 8%, and 2% of total Fe, respectively. Western blot analysis confirmed that these preparations contained some contaminating ER and vacuolar proteins (Fig. 4). The density of blots obtained using antibodies that bind to proteins in the ER, vacuoles, and cytosol was normalized using antibodies for the porin protein that localizes to mitochondria. We found that the normalized blot densities for contaminating organelles were *not* correlated to the % of the NHHS Fe^{II} doublet (Fig. 4, table). Similar analyses performed on 8 different batches of mitochondria isolated from glucose-grown cells also showed no correlation (Fig. S5). These results indicate that the NHHS Fe^{II} ions present in chelator-washed mitochondria are contained within these organelles rather than in contaminating membranous species such as ER or vacuoles.

Dithionite- and deoxycholate-treated mitochondria

We also used deoxycholate in the presence of the reductant dithionite to evaluate whether the HS Fe^{III} species in our mitochondrial samples were contained within the organelle. We treated half of a WT EGTA-washed fermenting mitochondria sample with dithionite; the other half was treated with dithionite and deoxycholate.

The low-field spectrum of the dithionite-and-deoxycholate treated sample (Fig. 5A, black hashmarks) contained a doublet due to Fe^{II}EGTA with $\delta = 1.3$ mm/s, $\Delta E_Q = 3.6$ mm/s (Fig. 5A, blue line) that represented 40% of the total Fe. The corresponding spectrum of the dithionite treated sample exhibited a NHHS Fe^{II} doublet with about half that intensity (Fig. 5A, blue line). The deoxycholate treated-minus-untreated difference spectrum (Fig. 5B) revealed that besides EGTA coordination to the 20% of NHHS Fe^{II} species originally in the dithionite-treated sample, ~ 20% of the Fe from other species was also converted to Fe^{II}(EGTA). High field spectra (Fig. S6) reveal that some (~ 12% of total Fe) of these other species originated from HS mononuclear Fe^{III} species. Spectral features from such species are evident in the 8.0 T spectrum of the dithionite-treated sample but absent in that of the dithionite-plus-deoxycholate-treated sample. The other iron species contributing to the Fe^{II}(EGTA) complex (~ 8% of total Fe) could not be identified, but they could be Fe^{III} nanoparticles. The central doublet contribution was unchanged in the experiment, consistent with deoxycholate treatment being gentler than sonication in disrupting membranes but not damaging Fe₄S₄ clusters. These results suggest that the mononuclear HS Fe^{III} species (and perhaps Fe^{III} nanoparticles) that contribute to the spectra of isolated fermenting mitochondria are contained within these organelles, protected from reduction by dithionite. Disruption of these membranes by deoxycholate removed this protection, allowing dithionite to reduce Fe^{III} to Fe^{II}. EGTA then chelated the Fe^{II} ions forming the observed Fe^{II}(EGTA) doublet.

Whole yeast cells

^{57}Fe -enriched whole fermenting yeast cells exhibited 4.5 K Mössbauer spectra dominated by features indicating magnetically non-interacting mononuclear HS Fe^{III} components (Fig. 6). These components have vanishingly small spin-dipolar interactions with other paramagnetic Fe sites. At 0.05 T (Fig. 6A), they display paramagnetic hyperfine structure (a quadrupole doublet would be expected if spin-dipolar interactions were effective or if the Fe^{III} component belonged to nanoparticles with a $T_B \ll 4$ K). At 8.0 T (Fig. 6C), such species exhibited patterns characteristic of magnetically non-interacting Fe^{III} . This behavior implies that these components should be EPR active.

The red lines in Fig. 6 are the sum of simulations for three mononuclear HS Fe^{III} species, collectively representing ~75% of spectral intensity; the actual number of species contributing to these features remains undetermined. Individual differences amongst the HS Fe^{III} species are lost at 8.0 T. The difference spectrum (Fig. 6B) obtained by subtracting the low-field simulation of Fig. 6A from the spectrum of Fig. 6A is similar to that obtained for isolated mitochondria (the blue line in Fig. 6B is the spectrum of EGTA-washed mitochondria shown in Fig. 1A).

A detailed analysis of the iron content of entire yeast cells will require a separate analysis, but our current analysis is sufficient for us to draw two major conclusions. First, the magnetically non-interacting mononuclear HS Fe^{III} species (whose contribution was removed from the spectrum of Fig. 6A) are *not* located in mitochondria. Second, the majority of Fe in fermenting yeast cells can be divided into two major groups – these non-mitochondrial mononuclear Fe^{III} species and mitochondrial Fe.

The non-mitochondrial Fe^{III} species are reduced to the Fe^{II} state upon sonication of cells and treatment with dithionite (Fig. S7). The resulting quadrupole doublet had $\Delta E_Q = 3.10$ mm/s and $\delta = 1.35$ mm/s, parameters similar to those of the NHHS Fe^{II} doublet in isolated mitochondria. This does not necessarily mean that the two doublets represent the same pool of iron, but neither can this possibility be excluded.

Discussion

NHHS Fe^{II} pool within isolated mitochondria

The major conclusion of this study is that the NHHS Fe^{II} species that are present in our isolated mitochondrial samples are located *within* the organelle. Three lines of evidence support this. Firstly, such species were observed after intact mitochondria were exposed to high concentrations of strong Fe^{II} chelators (EGTA and BPS) for extensive periods of time. EGTA is reported not to penetrate mitochondrial membranes and BPS is unlikely to do so because of its negative charge. We have observed such species in all ~30 batches prepared in this way over the course of the past 5 years. These Fe^{II} species were present in samples that had not been sonicated or exposed to phen, indicating that they were not generated by the degradation of $[\text{Fe}_4\text{S}_4]$ clusters.

Secondly, BPS and EGTA were only able to coordinate NHHS Fe^{II} *after* samples were sonicated. As sonication disrupts mitochondrial membranes, we conclude that the NHHS Fe^{II} species are located within the mitochondria and are *protected* from these chelators until the mitochondrial membranes are disrupted by sonication or by detergents such as deoxycholate. This conclusion is supported by the observation that phen (with a similar coordinating chemical structure as BPS but neutral and membrane permeable) can chelate the NHHS Fe^{II} species without sonication.

Thirdly, there was no correlation between the spectral intensity of the NHHS Fe^{II} doublet and the level of ER or vacuolar contamination in our samples. This excludes the possibility that these Fe^{II} species are located in a membrane-bound but non-mitochondrial organelle that contaminated our preparations.

Other scenarios have also been considered. For example, it is conceivable that during isolation, mitochondrial membranes become more permeable, allowing Fe from the isolation buffers to enter into the organelle. However, in this case, one would also expect that the strong chelators present in these buffers would have also entered the organelle and coordinated the observed HS Fe^{II} species, and/or that Fe within the organelle would also diffused into the buffer, draining the organelle of the observed HS Fe^{II}. The presence of the HS Fe^{II} species argues against these scenarios.

These Fe^{II} components represent ~ 20% of the total Fe in the organelle (700 – 800 μ M), corresponding to *ca.* 150 μ M in NHHS Fe^{II}. Given the low intensity of our signals and batch-to-batch variations, we estimate an overall relative uncertainty of \pm 30% (100 – 200 μ M) for the concentration of these components in fermenting mitochondria. This concentration is an order-of-magnitude higher than previous estimates based on fluorescence studies. Comparing results is difficult because the sources of the mitochondria (yeast *vs.* rat liver) differed as is the metabolic conditions under which the cells were prepared. Nevertheless, our studies show that the concentration of these ions in mitochondria isolated from fermenting yeast is higher than has been generally assumed.

Other pools of iron in mitochondria and whole cells

Although the focus of this paper was to establish whether the NHHS Fe^{II} species were located within yeast mitochondria, our experiments also provide evidence for other pools of Fe in the organelle, including Fe^{III} nanoparticles (~ 40% of Fe, corresponding to ~ 300 μ M, but somewhat variable) and mononuclear HS Fe^{III} ions (~ 20% of Fe, corresponding to ~ 150 μ M). The combined concentration of these three pools (600 μ M) represents ~ 80% of the total Fe in fermenting mitochondria. This is again a larger-than-expected proportion of mitochondrial Fe in the form of Fe pools. Whether these pools are independent of each other (e.g. imported through different IM transporters) or are in dynamic equilibrium with each other is unknown, but we assume the latter in the model of Figure 7. We have also observed a fourth pool of Fe in fermenting yeast cells, namely mononuclear HS Fe^{III} ions located in a non-mitochondrial region of the cell. The concentration of this pool is high, representing ~ 75% of all Fe in the cell.

We have not established the metabolic role of any of these pools. Fe^{II} ions are imported into the mitochondrial matrix via two high-affinity transporters (Mrs3p/Mrs4p), and this pool is used as feedstock for Fe/S and heme biosynthesis. Studies also suggest the presence of an Fe^{III} pool in vacuoles (23). It is appealing to consider that we have observed these and perhaps other Fe pools in yeast, but further studies are required to establish this. Mössbauer spectroscopy in combination with the analysis of various genetic strains of yeast will undoubtedly be useful in elucidating this and other details of iron trafficking in cells.

Supplementary Material

Refer to Web version on PubMed Central for supplementary material.

Abbreviations

LS low-spin

HS	high-spin
NHHS	nonheme high-spin
BPS	bathophenanthroline sulfonate
EGTA	glycol-bis(2-aminoethylether)-N,N,N',N'-tetraacetic acid

References

1. Atamna H. Heme, iron, and the mitochondrial decay of ageing. *Ageing Research Reviews* 2004;3:303–318. [PubMed: 15231238]
2. Mühlenhoff U, Stadler JA, Richhardt N, Seubert A, Eickhorst T, Schweyen RJ, Lill R, Wiesenberger G. A specific role of the yeast mitochondrial carriers Mrs3/4p in mitochondrial iron acquisition under iron-limiting conditions. *J. Biol. Chem* 2003;278:40612–40620. [PubMed: 12902335]
3. Shvartsman M, Kikkeri R, Shanzer A, Cabantchik ZI. Non-transferrin-bound iron reaches mitochondria by a chelator-inaccessible mechanism: Biological and clinical implications. *American Journal of Physiology-Cell Physiology* 2007;293:C1383–C1394. [PubMed: 17670894]
4. Lesuisse E, Santos R, Matzanke BF, Knight SAB, Camadro JM, Dancis A. Iron use for haeme synthesis is under control of the yeast frataxin homologue (Yfh1). *Human Molecular Genetics* 2003;12:879–889. [PubMed: 12668611]
5. Tangeras A, Flatmark T, Backstrom D, Ehrenberg A. Mitochondrial iron not bound in heme and iron-sulfur centers - estimation, compartmentation and redox state. *Biochim. Biophys. Acta* 1980;589:162–175. [PubMed: 6243966]
6. Petrat F, de Groot H, Sustmann R, Rauen U. The chelatable iron pool in living cells: A methodically defined quantity. *Biol. Chem* 2002;383:489–502. [PubMed: 12033438]
7. Petrat F, Weisheit D, Lensen M, de Groot H, Sustmann R, Rauen U. Selective determination of mitochondrial chelatable iron in viable cells with a new fluorescent sensor. *Biochem. J* 2002;362:137–147. [PubMed: 11829750]
8. Miao R, Martinho M, Morales JG, Kim H, Ellis EA, Lill R, Hendrich MP, Munck E, Lindahl PA. EPR and Mössbauer spectroscopy of intact mitochondria isolated from yah1p-depleted *Saccharomyces cerevisiae*. *Biochemistry* 2008;47:9888–9899. [PubMed: 18717590]
9. Hudder BN, Morales JG, Stubna A, Münck E, Hendrich MP, Lindahl PA. Electron paramagnetic resonance and Mössbauer spectroscopy of intact mitochondria from respiring *Saccharomyces cerevisiae*. *Journal of Biological Inorganic Chemistry* 2007;12:1029–1053. [PubMed: 17665226]
10. Diekert K, de Kroon AIPM, Kispal G, Lill R. Isolation and subfractionation of mitochondria from the yeast *Saccharomyces cerevisiae*. *Methods in Cell Biology* 2001;65(65):37–51. [PubMed: 11381604]
11. Stevens BJ. Variation in number and volume of mitochondria in yeast according to growth-conditions - study based on serial sectioning and computer graphics reconstitution. *Biologie Cellulaire* 1977;28:37–56.
12. Lindahl, PA.; Morales, JG.; Miao, R.; Holmes-Hampton, G. *Methods enzymol.* Academic Press; 2009. Chapter 15 isolation of *Saccharomyces cerevisiae* mitochondria for Mössbauer, EPR, and electronic absorption spectroscopic analyses; p. 267-285.
13. Luo Y, Bond JD, Ingram VM. Compromised mitochondrial function leads to increased cytosolic calcium and to activation of map kinases. *Proc. Natl. Acad. Sci. U. S. A* 1997;94:9705–9710. [PubMed: 9275188]
14. Dickson, DPE.; Berry, FJ. *Mössbauer spectroscopy.* Cambridge University Press; Cambridge; New York: 1986.
15. Wikstrom M, Krab K, Saraste M. Proton-translocating cytochrome complexes. *Annu. Rev. Biochem* 1981;50:623–655. [PubMed: 6267990]
16. Kent TA, Münck E, Dunham WR, Filter WF, Findling KL, Yoshida T, Fee JA. Mössbauer study of a bacterial cytochrome-oxidase - cytochrome c1aa3 from *Thermus-thermophilus*. *J. Biol. Chem* 1982;257:2489–2492.

17. Miao R, Kim H, Koppolu UMK, Ellis EA, Scott RA, Lindahl PA. Biophysical characterization of the iron in mitochondria from Atm1p-depleted *Saccharomyces cerevisiae*. *Biochemistry* 2009;48:9556–9568. [PubMed: 19761223]
18. Garber-Morales J, Holmes-Hampton GP, Miao R, Guo Y, Münck E, Lindahl PA. The iron-ome of mitochondria isolated from respiring and fermenting *Saccharomyces cerevisiae*. 2010
19. Flatmark, T.; Tangeras, A. Mitochondrial ‘non-heme non-FeS iron’ and its significance in the cellular metabolism of iron. In: E.B. Brown, PA.; Fielding, J.; Crichton, RR., editors. *Proteins of iron metabolism*. Grune & Stratton; New York, USA: 1976. p. 349-358.
20. Glick BS, Pon LA. Isolation of highly purified mitochondria from *Saccharomyces cerevisiae*. *Mitochondrial Biogenesis and Genetics* 1995;(Pt A 260):213–223.
21. Goetz JG, Nabi IR. Interaction of the smooth endoplasmic reticulum and mitochondria. *Biochem. Soc. Trans* 2006;34:370–373. [PubMed: 16709164]
22. Green DE, Tisdale HD, Criddle RS, Bock RM. Structural protein and mitochondrial organization. *Biochem. Biophys. Res. Commun* 1961;5:81. [PubMed: 13708168]
23. Singh A, Kaur N, Kosman DJ. The metalloreductase Fre6p in Fe-efflux from the yeast vacuole. *J. Biol. Chem* 2007;282:28619–28626. [PubMed: 17681937]

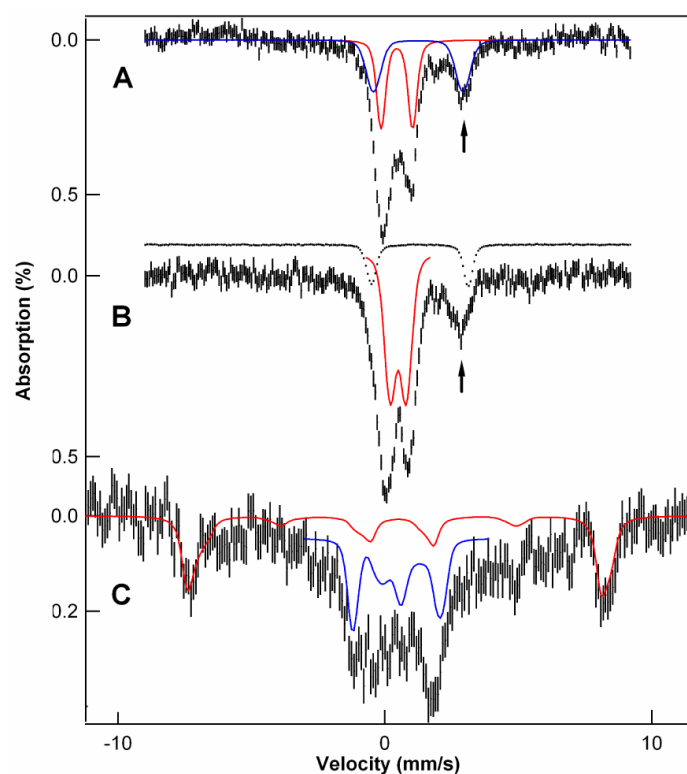


Figure 1.

Mössbauer spectra of EGTA-washed fermenting mitochondria (Sample F12, (18)) recorded at 4.5 K and 0.05 T (A), 100 K and 0.05 T (B), and 4.2 K and 8 T (C). Solid lines simulate the contributions of NHHS Fe^{II} species (blue line in A, ~20% of total Fe), the central doublet (red line in A and blue line in C, ~20%), Fe^{III} nanoparticles (red line in B, ~40%), and mononuclear HS Fe^{III} species (red line in C, ~20%). Shown offset above B is the experimental spectrum of Fe^{II} (EGTA) (black hashmarks). The black arrows in Figures 1-3 point to the high energy absorption line of the NHHS Fe^{II} species.

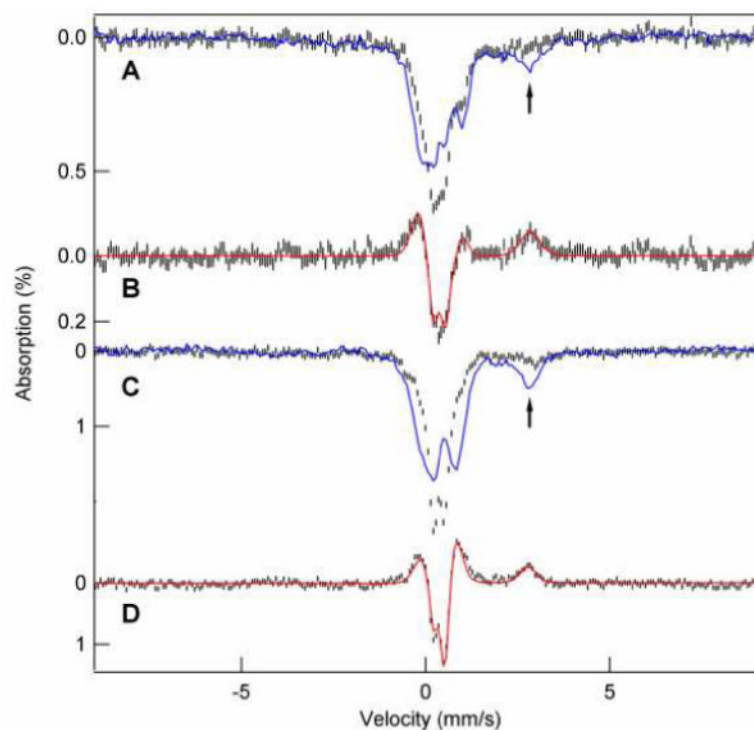


Figure 2.

Mössbauer spectra (4.5 K, 0.05 T) of BPS-washed mitochondria (Sample F6, (18)). A, before (blue line) and after (hashmarks) sonication; B, after minus-before difference spectrum; the red line in B is a simulation assuming that NHHS Fe^{II} and the central doublet Fe were converted into the $\text{Fe}^{\text{II}}(\text{BPS})_3$ complex. C and D are Mössbauer spectra (100 K, 0.05 T) of a second experiment using EGTA-washed mitochondria treated in the final step with BPS. C, (Sample F13, (18)) before (blue line) and after (hashmarks) sonication; D, after-minus-before difference spectrum. The red line is a simulation assuming that NHHS Fe^{II} (12% of total Fe), Fe of the central doublet (14% of total Fe) and Fe^{III} nanoparticles (34% of total Fe) were converted into $\text{Fe}^{\text{II}}(\text{BPS})_3$ (60% of total Fe).

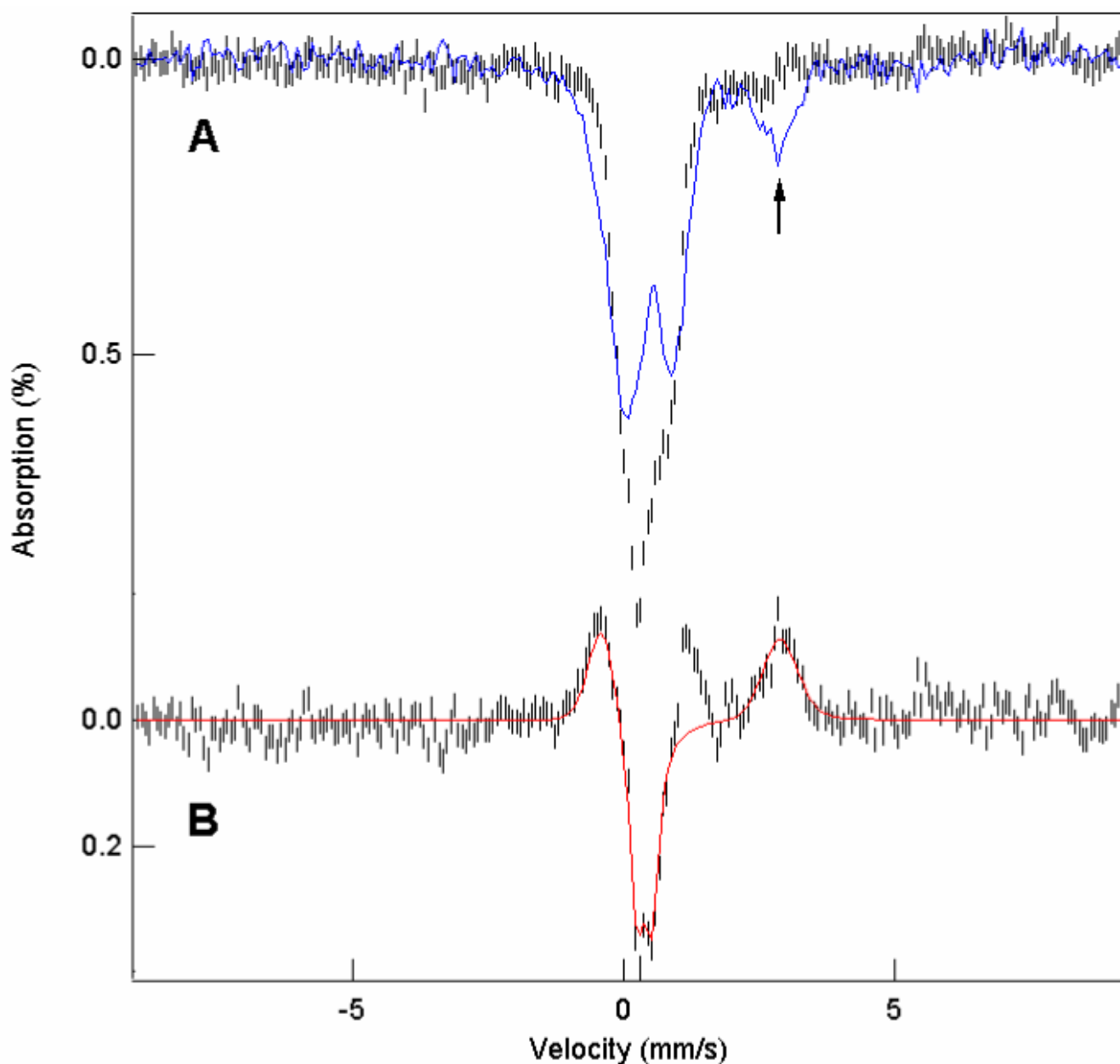
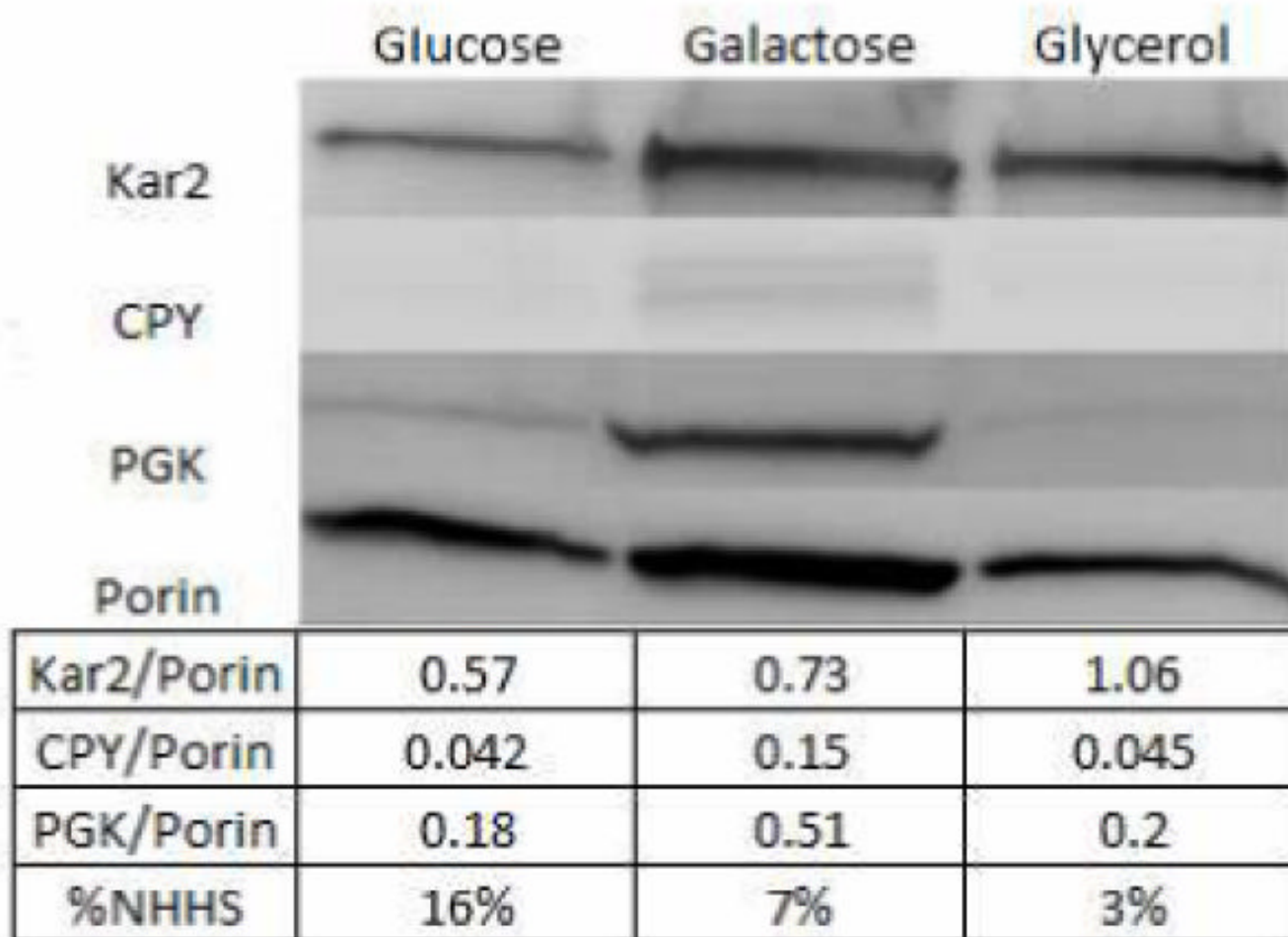


Figure 3. Mössbauer spectra (4.5 K 0.05 T) of EGTA-washed mitochondria (Sample F14, (18)) incubated (A, black hash marks), and not incubated (A, blue line) with phen. B, incubated-minus-not-incubated difference spectrum. The red line is a simulation assuming that NHHS Fe^{II} ions converted to $\text{Fe}^{\text{II}}(\text{phen})_3$ after exposure to phen. The remaining $\text{Fe}^{\text{II}}(\text{phen})_3$ doublet originated from either Fe^{III} nanoparticles, mononuclear Fe^{III} ions or irons of the central doublet.

**Figure 4.**

Western blot of extracts of mitochondria from cells grown on glucose (left lane), galactose (middle) and glycerol (right) (Samples F5, RF1 and R1(18)). For each sample, 60 μ g of protein, determined by the bicinchoninic acid method (Thermo Scientific), was added to each lane of a 10% SDS-PAGE gel. Primary antibodies used in staining included Kar2p, CPY, PGK, and porin. Integrated intensities of contaminating bands were normalized to the intensity of the corresponding porin band. These ratios are given in the table along with the percentage of the NHHS Fe^{II} doublet observed in the Mössbauer spectrum of the same material.

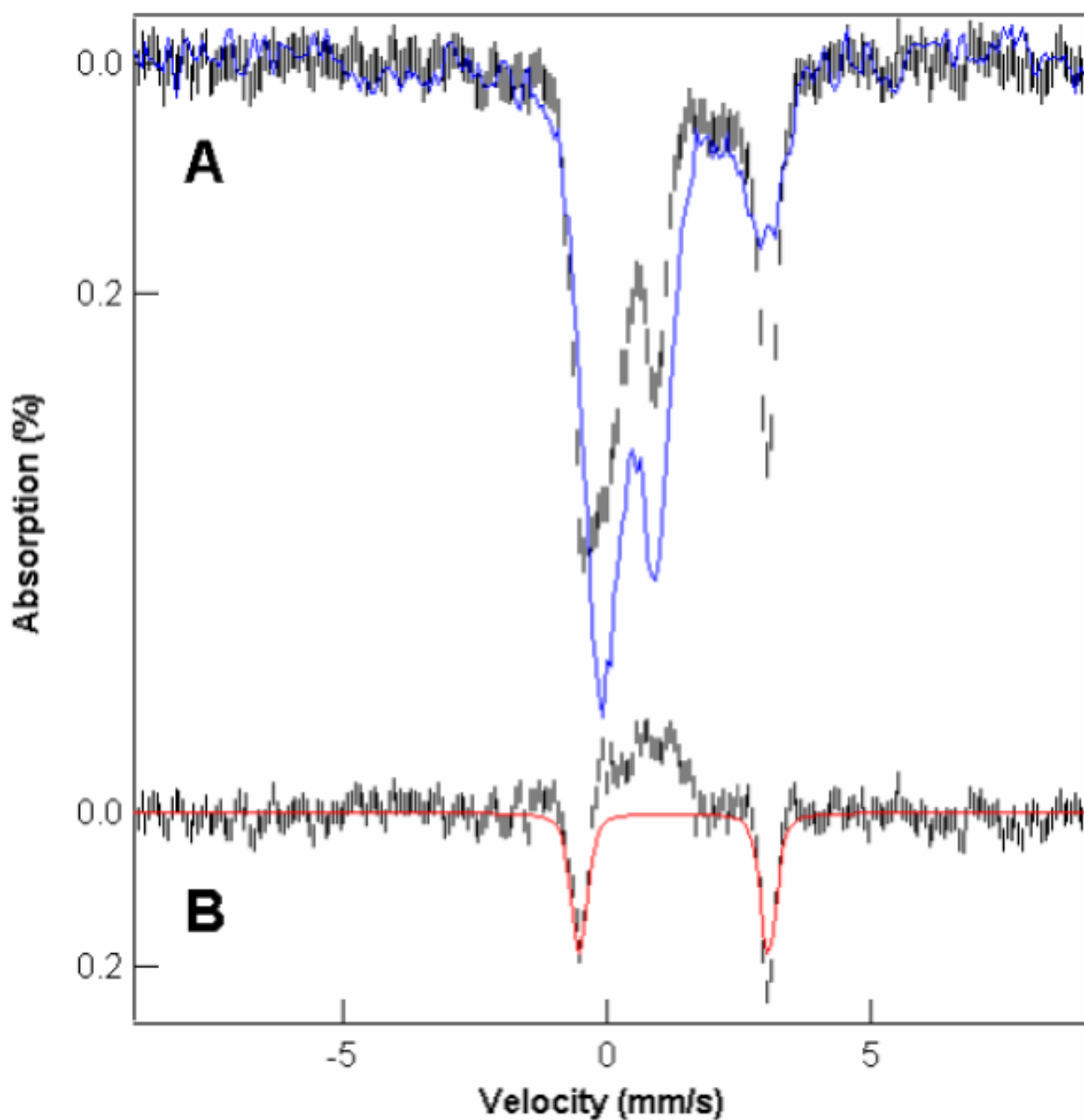


Figure 5.

Effect of deoxycholate on the ability of dithionite to reduce Fe^{III} species in EGTA-treated mitochondria (Sample F15, (18)). A, 100 K Mössbauer spectra of EGTA-washed, dithionite-treated, mitochondria in the absence (blue) and presence (black hashmarks) of deoxycholate. B, presence-minus-absence of deoxycholate difference spectrum; the red line is a simulation representing 20% of total Fe with $\delta = 1.3$ mm/s, $\Delta E_Q = 3.6$ mm/s.

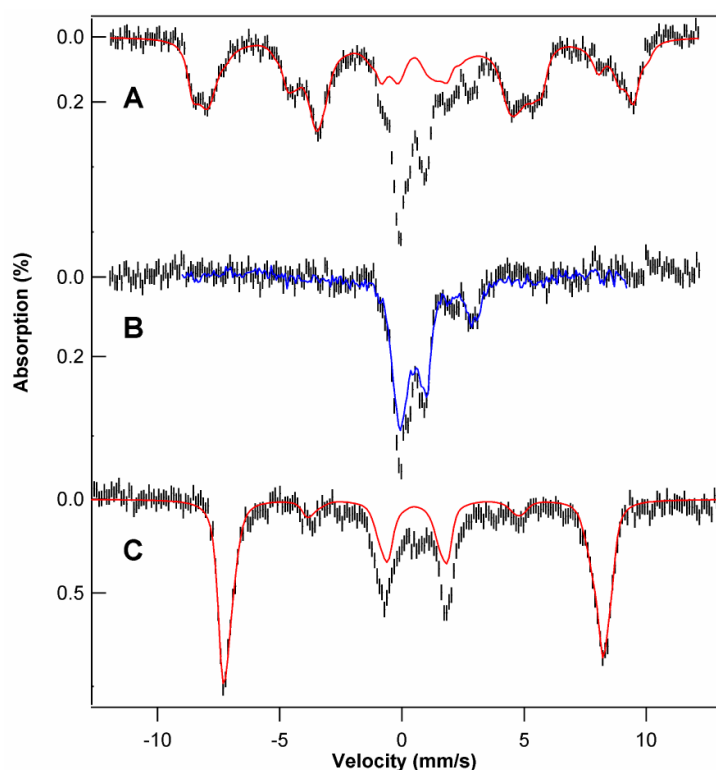


Figure 6.

4.5 K Mössbauer spectra of whole fermenting yeast cells grown on ^{57}Fe -enriched minimal media. A, 0.05 T applied field. The red line is a simulation with A values ranging from -21 T to -23.5 T. B, spectrum obtained after subtracting the simulation in A from the data; the blue line is the spectrum of isolated mitochondria given in Fig. 1A. C, same as A, but at 8.0 T applied field; the red line is a simulation with A values ranging from -21.5 T to -22.5 T.

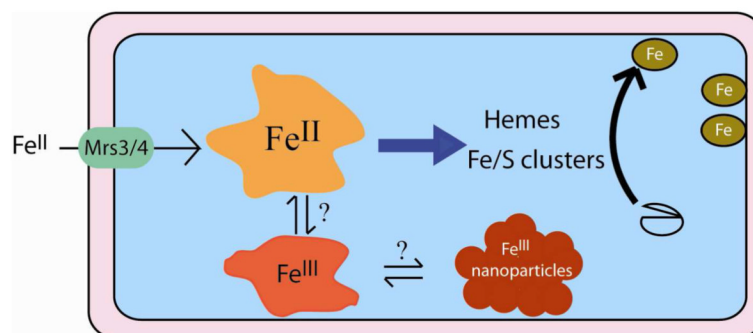


Figure 7. Distribution of iron pools in mitochondria isolated from fermenting yeast. Three pools composed of nonheme HS Fe^{II} species, mononuclear HS Fe^{III} species, and Fe^{III} nanoparticles have been identified.